Biomechanical comparison of plate materials and designs for subcondylar fracture fixation: An *in silico* assessment

Anoushka Gupta[1,2], Abir Dutta[1,3], Kaushik Dutta[4], Kaushik Mukherjee[1*]

[1]Department of Mechanical Engineering, Indian Institute of Technology Delhi, Hauz Khas, New Delhi – 110016, India

[2]Department of Mechanical Engineering, Johns Hopkins University, Baltimore, MD, 21218, USA

[3]Department of Ortho and MSK Science, University College London, UK

[4]Department of Oral Medicine and Radiology, Guru Nanak Institute of Dental Sciences and Research, Kolkata, India

*Corresponding author: kmukherjee@mech.iitd.ac.in

Abstract

The fixation of common mandibular subcondylar fractures is associated with a high complication rate, and the decision of a suitable plate design and material still remains a challenge. Computational models have been developed and verified for understanding mandibular fracture fixation, but most of the investigation has been limited to a simplified model, single force and evaluation of plate-only designs. Using finite elements, we analysed the fracture stability with five materials - Nitinol, Magnesium alloys, two types of Titanium alloys (Ti-6Al-4V and Ti-29Nb-13Ta-4.6Zr) and Stainless Steel 316L, for four types of fixation plate designs. The soft tissues such as periodontal ligament, were included and molar clenching tasks were considered for accurately mimicking the physiological mastication cycle. The maximum principal tensile strain in the mandible was found to be decreasing with an increase in stiffness for most of the cases, except for the trapezoid and strut plates. We attribute the differences between trapezoid/strut and double mini/lambda to the presence of an additional screw near the sigmoid notch in the proximal segment in case of double mini and lambda plates. As the mandible reconstructed with double mini plates had the least interfragmentary gap, the double mini plate was deemed as the most suitable design. The results such as a lower von Mises stress in plates (compared to yield strength) indicated that the anchorage provided by titanium alloys (Ti-6Al-4V and TNTZ) is sufficient for load bearing.

Keywords: finite element, *in silico*, masticatory cycle, mandible, fracture plate, subcondylar fixation

1. Introduction

The subcondylar region of mandible is one of the most common facial fractures [1][2], majorly as a consequence of vehicular accidents or interpersonal violence. Presently, Open Reduction and Internal Fixation (ORIF) is used to treat mandible fractures [3]. However, ORIF has a 10-30% complication rate resulting in secondary surgeries and, thereby, increase in financial burdens [4]. The narrow anatomy and unique physiology of subcondylar fractures make the fixation extremely challenging. The choice of material and geometric configuration of the fixation plate determines the outcome of the surgery. For favourable patient outcomes, the stiffness and the density of the implant material should align with the properties of native bone tissue, and the geometric configuration should support the load transfer in the narrow subcondylar region. Recently, three-dimensional plates such as Trapezoid, Strut and Lambda plates were designed specifically for subcondylar fractures [5]. In addition, the use of double mini plates has also garnered support to provide stability in a fixation [6].

Although there are different types of clinically approved materials, the Ti-6Al-4V alloy is considered the gold standard due to its favourable biomechanical strength and biocompatibility. However, Ti-6Al-4V has higher elastic modulus as compared to the cortical bone [7], which leads to detrimental implications such as stress shielding, resulting in an implant-removal rate of 10-12% [8]. Another metallic material, Steel (AISI SS 316L), has been popularly used due to its affordability but has two times higher density (8.1-8.9 g/cm^3) as compared to titanium (4.4-4.5 g/cm^3) as well as a higher modulus of 210 GPa [8, 9]. In addition, these common metallic alloys are prone to corrosion, such as pitting, crevice corrosion and corrosion-induced cracking [10]. To overcome these issues, new alloys are being developed by including non-cytotoxic elements such as Niobium (Nb), Zirconia (Zr) and Tantalum (Ta) to reduce modulus and impart anti-corrosion ability. One such alloy which has been used for fracture fixation plate is Ti-29Nb-13Ta-4.6Zr (aged) with bio-inertness [11] and lower modulus of 80 GPa [12] (as compared to 110 GPa of Ti-6Al-4V [13]).

The alternative materials, such as Mg WE43 alloy (Mg-3.5Y-2.3Nd-0.5Zr), have a lower elastic modulus (44.2 GPa [14]) favouring neo-bone growth and integration [8]. Further advantages of Mg include low densities (1.74-2.0 g/cm^3 [8]) and abundant presence of Mg^{2+}

cation in the body [7]. MgWE43 alloy has an appropriate biodegradation rate for preventing non-union [15]. Another popular material being used in clinics for orthodontic braces is solid nitinol (NiTi), owing to its excellent biocompatibility, mechanical properties, and resistance to corrosion [16]. Furthermore, nitinol has less modulus (38.5 GPa [17]), which makes it a suitable choice for mandibular fracture fixation plates [18].

The finite element analysis (FEA) technique has become a preferred method to assess the feasibility of fixation methods suitable for subcondylar fractures [19]. However, the influence of different materials, such as nitinol and less rigid Ti alloy and designs, has not been extensively studied. Moreover, recent studies on three designs and two materials [20], and double mini plates with four materials [21] used simplified FE models under idealised loading conditions without consideration of soft tissues Hence, we developed a FE model with periodontal ligament, condylar fibrous tissues, teeth, cancellous and cortical and simulated under a complete mastication cycle as a part of our earlier study [22, 23]. However, our previous study [22] evaluated only Titanium implants and the influence of other implant materials was not considered. This study uses the published mandibular FE model methodology [22] to further analyse the influence of both designs and materials of implants on the reconstruction.

This study aims to gain an insight into the interplay of material properties and plate design on parameters such as interfragmentary distance at the fracture site that indicates fixation stability. Specifically, in this study, a comparative biomechanical evaluation of subcondylar fixation has been carried out for the following combinations of five different implant materials, namely Nitinol, Magnesium Alloy WE43, a low rigidity Titanium Alloy (TNTZ: Ti–29Nb–13Ta–4.6Zr), a common Titanium Alloy (Ti-6Al-4V) and Stainless Steel (SS 316L) and four implant designs, namely trapezoid, strut, lambda and double mini plates.

2. Materials and Methods

Anonymized computed tomography (CT) images with a pixel resolution of 512×512, pixel size of 0.439 mm and slice thickness of 0.75 mm of a healthy subject were obtained for the development of the intact mandible model. A virtual fixation with four plates was performed on the modelled fractured mandible. Thereafter, the plates were assigned with four different effective material properties, to investigate the influence of the materials on the load-transfer

across the mandible. The methodology used for the development of the intact and reconstructed mandibles has already been discussed in detail elsewhere [22] and, therefore, is briefly presented here.

2.1. Development of 3D model of intact mandible

The three-dimensional model (Figure 1a) of the mandible was developed based on the anonymised computed tomography (CT) dataset of a 20-year-old healthy male. Prior consent was taken from the participant at Guru Nanak Institute of Dental Sciences and Research, India. The data has been further anonymized for research purpose. The segmentation of the mandible into five different components (Cortical and cancellous bone, teeth, periodontal ligament (PDL) and fibrocartilage) was performed in Mimics 24.0 (Materialise, Leuven, Belgium). All the solid models of components, including the soft tissues, were discretized with a 10-noded tetrahedral element (SOLID 187) [24]. A 0.2 mm thick PDL layer was included due to the notable impact of the PDL on the load transfer from the teeth to the bone [22, 25]. Two blocks representing the temporal bone were modelled with 20x15x15 mm^3 having a concave depression [25, 26]. The condylar fibrocartilage, a soft tissue layer of 0.3 mm thickness, was attached to the depression [25, 26]. A mesh convergence study was performed and mesh sizes were chosen for the model having <1% deviation in the state of stresses and strains [22]. Based on the mesh convergence study for the same intact mandible FE model, [22], an element size of 0.2 – 1 mm was chosen.

2.2. Development of implanted mandible

A standardized osteotomy line [27] for subcondylar fracture, from the mid-point of the ramus to the bottommost point of sigmoid notch, was simulated in 3-Matic 16.0 (Materialise, Leuven, Belgium). Based on our earlier studies on five plate designs (single mini plate, trapezoid, strut, lambda and double mini), we chose four plate designs excluding single mini plate (Figure 1b) [22, 23]. Evidently, the single mini has been reported to have a high complication rate up to 33% [28, 29], corroborating our evaluation that it had insufficient fixation stability due to a very high interfragmentary displacement and high von Mises stress [22, 23]. Rest of the patient-specific plate designs used were inspired from the commercially

available plate designs (DePuy Synthes, PA). The screws were modelled as cylinders with diameter of 2 mm and length of 6 mm [30]. No relative movement was allowed between the screw and the plate representing all the screws as cold-welded locking screws. The double mini plates were fixed in an angulated manner [27] and the trapezoid, strut and lambda plates were fixed based on the recommended guidelines [5]. All the reconstructed mandibles consisted of a similar number of elements (~14,00,000) following a similar methodology of meshing with 10-noded tetrahedral elements, as the intact mandible.

2.3. Material Properties

Cancellous bone was assigned with voxel-based non-homogeneous isotropic properties. For each element, the apparent density (ρ) was calculated corresponding to its gray-scale value (in HU) following the relationship [22]:

$$\rho = \rho_1 + \frac{\rho_2 - \rho_1}{HU_2 - HU_1}(HU - HU_1) \quad (1)$$

where (ρ_1, HU_1) represented the no-bone condition (0.022 g/cm^3, 0 HU) and (ρ_2, HU_2) represented the hard-bone condition (1.73 g/cm^3, 2600 HU). The negative densities corresponding to <0 HU were flushed to the minimum values corresponding to the no-bone condition [31-33]. A power law relationship was used to calculate the element-specific Young's modulus of cancellous bone based on its apparent density [22, 34].

Cortical bone was assigned with region-specific orthotropic properties based [13, 22]. The rest of the structures, including the plates and screws were modelled as homogenous linear isotropic [13]. The teeth were further divided into enamel and dentin with different isotropic material properties [13]. Table 1 provides a summary of the material properties assigned to each component. The plates were assigned five different material properties as presented in Table 2 [9, 12-14, 17]. Titanium alloy (Ti-6Al-4V) properties (E = 110 GPa, ν = 0.3) [13] were assigned to the screws in all the cases.

2.4. Applied loading and boundary conditions

All the intact and reconstructed mandibles were simulated under the contralateral left unilateral molar clenching (LMOL) and the ipsilateral right unilateral molar clenching (RMOL).

These two load cases were chosen based on the reported maximum solicitation among a total of six load cases which form the complete mastication cycle 'alternating bilateral clenching pattern' [35, 36]. In addition, simulating the molar clenching tasks enabled the comparison of the clenching sides - each constituting following 7 muscles: superficial and deep masseter muscles (SM and DM), medial and inferior lateral pterygoid (MP and ILP), and anterior, middle, and posterior temporalis (AT, MT and PT) [13]. The magnitude of the force was distributed over the nodes representing the attachment sites of the corresponding muscles [13]. The top surfaces of the blocks, serving as the temporal bone, were fixed during the clenching tasks [13].

A standard frictional contact pair was defined with a frictional coefficient of 0.4 [22, 37, 38] at the plate-cortical and fracture interfaces. Rest of the surfaces between the adjacent parts, such as the screw with the plate, cancellous and cortical, were modelled as bonded. An augmented Lagrangian was employed to solve the contact pair.

2.5. Verification and Interpretation of results

As the CT scan was from a living subject, direct one-to-one experimental validation of the FE model was not possible. Nevertheless, the maximum principal strains and stresses in the intact mandible during a right molar clenching were found to be of quantitatively similar magnitude (~1200 $\mu\varepsilon$) at qualitatively similar regions as reported in literature [25]. Moreover, the reaction force generated at the constrained right molar teeth was ~850 N for the intact mandible during the right unilateral molar clenching task, that is within the range of occlusal forces for healthy humans (365 - 1230 N) [39]. Also, the direction of the overall deformation was found to be towards the working (chewing) side, as found in earlier reports [25, 40]. Hence, the reliability and accuracy of the FE modelling methodology were verified and adopted for all the reconstructed mandibles.

The maximum principal tensile strains and stresses were calculated for the reconstructed mandibles to evaluate the efficacy of devices and safety towards risk of non-union and secondary fractures. The equivalent von Mises stresses of the plates were calculated to predict the failure of ductile plate materials. 95th percentile values of all the generated stresses and strains were calculated to exclude singularities around the constrained regions. In addition, the

interfragmentary distance (Figure 1c) at the osteotomy site was also calculated to understand the stability of the fixation.

3. Results

The principal stresses, strains and equivalent von Mises stresses in the cortical bone and implants, respectively, are presented below. Further, different gaps created at the fracture site due to influence of chewing laterality, fixation design and material are discussed. Only the equivalent von Mises stress distributions in the plates have been presented in detail, whereas the results for the screws are presented in the supplementary data.

3.1. Principal tensile stress and strain in the mandible

The maximum principal tensile stresses in the intact mandible were found on the buccal border below the right or left molar teeth under RMOL (14.8 MPa) or LMOL (14.1 MPa) respectively (Figure 2). The maximum tensile stresses in all the reconstructed mandibles (15-18 MPa) were higher as compared to the intact mandible. However, the different material properties of plates resulted in minimal differences (± 0.2-0.5 MPa) in maximum principal stresses in the reconstructed mandibles (Table S1). But among different plate designs, highest maximum principal tensile stresses (~18 MPa under RMOL, ~16 MPa under LMOL) were observed in the mandible reconstructed with trapezoid plate. Lowest tensile stresses in the reconstructed mandibles were found with the lambda plate (~16.9 MPa) under RMOL and strut plate (~15 MPa) under LMOL.

The maximum principal tensile strains (1288 με under RMOL and 1240 με under LMOL) occurred along the anterior border near the condyle and coronoid of intact mandible (Figure 2). In reconstructed mandibles, there were higher strain values (1383 - 1635 με) than those observed in the intact mandible. An increase in the stiffness of the plates resulted in varying trends of strains in the reconstructed mandibles for different plate designs and clenching sides. For all plates under RMOL, the strains in the reconstructed mandibles reduced with an increase in the stiffness of the plates (Table 5). Under LMOL, this trend was followed by only lambda and double mini plates, and the strut and trapezoid plates resulted in the opposite trend of increasing

strains in reconstructed mandibles with increasing stiffness (Table 5). Among all plate designs, the strut plate resulted in the least maximum tensile strain in reconstructed mandibles for most of the cases, with values ranging between 1522-1541 με under RMOL, 1383-1429 με under LMOL The lambda plate has resulted in the least maximum tensile strain (1402 με) for SS 316L plate material and LMOL load case.

3.2. Stress distributions in Implants

The maximum von Mises stresses in the plate were found to be increasing with increase in modulus of the fixation plates (Table 3 for titanium (both Ti-6Al-4V and TNTZ) fixation plates, the maximum von Mises stresses did not exceed the yield strength for all designs. For nitinol, only the strut plate resulted in lower von Mises stress than the yield strength. Whereas for Mg WE43 and SS316L materials, all the plates exhibited maximum von Mises stresses beyond the yield limit. A marginal increase in von Mises stresses was found in the posterior part of the plates under RMOL (Figure 3). It was observed that there is a higher stress distribution in the anterior arm of the trapezoid plate under LMOL (Figure 4). The maximum von Mises stresses in the screws were in the range 132 - 170 MPa under RMOL, and 170 - 304 MPa under LMOL with details present in the supplementary data (Table S3-4-6 and Figure S1-2).

3.3. Interfragmentary Distance

For all plate designs and load cases, the interfragmentary distances were found to be decreasing with increase in stiffness of fixation plates (Table 4). Interfragmentary distance was defined as a relative displacement between two bone segments on both sides of the fracture line (Figure 1c). Among all plate designs, the least interfragmentary distance was found with the double mini plate for all the load cases and material properties. For the trapezoid and strut plate, different material properties of plates had resulted in different trends of variation of interfragmentary distance with the clenching side. However, for lambda and double mini plates, the trend (higher or lower under RMOL than under LMOL) was consistent with all the material properties.

4. Discussion

It is important to clarify that the implant requires sufficient strength to sustain functional requirements and avoid unfavourable outcomes of the surgery. Our study focused on an *in silico*

assessment of four plate designs with different materials for subcondylar fracture fixation under mastication forces. All the biological structures including the PDL and condylar fibrous tissue were modelled aiming at a rigorous evaluation of the safety of the plates. Despite rigorous nature of the study, it has few limitations. Although heterogeneous material properties were assigned to the cancellous bone and orthotropic material properties were assigned to the cortical bone, the model lacks simulation of the non-linear nature of nitinol and heterogeneous anisotropic properties for the cortical bone. Also, this study does not consider inter-patient variability due to differences in morphological properties such as bone density and volume, so the results should be considered as patient-specific. The models also lack the actual representation of the screws with detailed threads. The influence of screw placement is another factor that could influence fixation stability. However, that investigation was out of the scope of the present study.

Limitations notwithstanding, the FE modelling methodology was verified with the literature based on the overall consistency with the results in the literature, such as the maximum principal stresses (15 MPa vs 20 MPa [25]) and the locations of the high stresses near the alveolar region of the mandible. The maximum principal tensile strains were also found comparable to the results reported earlier [25] for healthy bone. The maximum principal tensile strains for all the reconstructed mandibles were well below the yield strain limit (~2500 $\mu\varepsilon$) for the mandible in tension [41]. Under ipsilateral occlusion (RMOL), the constrained teeth are lied in the fracture plane, whereas under LMOL, the constrained teeth on the opposite side (Figure 5) resulted in the out-of-plane bending moment. Hence, as a result of this moment under contralateral occlusion (LMOL), all plate designs experienced more stress than when subjected to RMOL. Furthermore, in the mandibles subjected to RMOL, the mandibular strains decreased with increasing elastic modulus of plate as it provided increasing stability. This trend was also exhibited under LMOL but only for mandibles reconstructed with lambda and double mini plates as the presence of two anterior screws in the proximal segment provided high moment resistance and hence high stability (also proved by the least value of other parameters like mandibular tensile stress and interfragmentary distance). Whereas with trapezoid and strut plate, which provided relatively less moment resistance due to only one anterior screw in proximal segment, the increasing stability trend was not observed and the mandibular strains increased with increasing elastic modulus of plates. This trend of increasing mandibular strains was observed due to decreasing strains in the plates with increasing elastic modulus of plates (Table S3), as the

soft plates undergo more deformation than stiff plates, so the soft plates absorb higher amount of total strains leading to lower strains in the corresponding reconstructed mandibles.

For further evaluation of fracture reconstruction, the chance of failure of the reconstruction plate [42] was investigated based on the maximum von Mises stresses in the plates. As the maximum von Mises stresses in the SS316L and Magnesium plates were found to be exceeding the yield strength, SS316L and Magnesium should be used with caution due to a risk of plate failure. With nitinol, only the use of a strut plate is suggested based on low maximum von Mises stress, supporting the favourable performance of strut plate among all designs. Both the titanium alloys (Ti-6Al-4V and TNTZ) provide adequate strength with the resulting maximum von Mises stresses well below the yield limits. TNTZ plates, even with a lower modulus than Ti-6Al-4V, had a lower ratio of maximum von Mises stress with respect to the yield strength than Ti-6Al-4V under LMOL for all the plate designs.

In addition to the stresses and strains, we also evaluated another important indicator of stability of fracture fixation: interfragmentary distance. The observed reduction in the interfragmentary distances with a reduction in the stiffness of the implant materials, added support to the use of stiff materials and Ti alloys. The interfragmentary distance trend with material stiffness corroborated the results in literature [21]. However, in the design aspect, the double mini plates fixed with the highest number of screws, led to the most superior stabilisation [21]. Lambda plate resulted in a very high interfragmentary distance (beyond the critical limit of 150 μm [43, 44] for facilitating fracture healing) under RMOL, indicating the risk of non-union while using lambda plate. The strut plate and trapezoid plates had almost similar interfragmentary distances under RMOL and the interfragmentary distances did not exceed 150 μm in any of the cases. However, the double mini plates fixed with the highest number of screws, resulted in the lowest interfragmentary distance and least mandibular strains indicating that in terms of design, double mini design resulted in the most superior fixation.

5. Conclusion

A biologically realistic FE model was developed to evaluate fixation using different implant designs and materials during mastication. The different trends between plates with varying number of screws highlighted the importance of screws in the proximal segment to resist the

moment present under contralateral chewing. Based on the least strain in mandibles and the least interfragmentary distances, the double mini plates are suggested as the most optimal. Even though nitinol and Mg WE43 posed some advantages, they resulted in high equivalent von Mises stresses in plates, indicating that the use of titanium is more suitable. Our study suggests that the patients should continue with the intuitive contralateral chewing to prevent instability. The results from this study potentially aid in the development of improved fixation technique of double mini plates made of less rigid titanium alloys such as TNTZ.

References

1. Sukegawa, S., et al., *Which fixation methods are better between three-dimensional anatomical plate and two miniplates for the mandibular subcondylar fracture open treatment?* Journal of Cranio-Maxillofacial Surgery, 2019. **47**(5): p. 771-777.
2. Hedeșiu, M., et al., *Three-Dimensional Finite Element Analysis on Mandibular Biomechanics Simulation under Normal and Traumatic Conditions.* Oral, 2022. **2**(3): p. 221-237.
3. Abdel-Galil, K. and R. Loukota, *Fractures of the mandibular condyle: evidence base and current concepts of management.* British Journal of Oral Maxillofacial Surgery 2010. **48**(7): p. 520-526.
4. Nasser, M., et al., *Interventions for the management of mandibular fractures.* Cochrane database of systematic reviews, 2013(7).
5. Murakami, K., et al., *Computed Tomography–Based 3-Dimensional Finite Element Analyses of Various Types of Plates Placed for a Virtually Reduced Unilateral Condylar Fracture of the Mandible of a Patient.* Journal of Oral Maxillofacial Surgery, 2017. **75**(6): p. 1239. e1-1239. e11.
6. Wagner, A., et al., *A 3-dimensional finite-element analysis investigating the biomechanical behavior of the mandible and plate osteosynthesis in cases of fractures of the condylar process.* Oral Surgery, Oral Medicine, Oral Pathology, Oral Radiology, Endodontology, 2002. **94**(6): p. 678-686.
7. Anand, N. and K. Pal, *Evaluation of biodegradable Zn-1Mg-1Mn and Zn-1Mg-1Mn-1HA composites with a polymer-ceramics coating of PLA/HA/TiO2 for orthopaedic applications.* J Mech Behav Biomed Mater, 2022. **136**: p. 105470.
8. Prasadh, S., et al., *The Potential of Magnesium Based Materials in Mandibular Reconstruction.* Metals, 2019. **9**(3).
9. Xie, F., et al., *Structural and mechanical characteristics of porous 316L stainless steel fabricated by indirect selective laser sintering.* Journal of Materials Processing Technology, 2013. **213**(6): p. 838-843.
10. Jacobs, J.J., J.L. Gilbert, and R.M. Urban, *Current Concepts Review - Corrosion of Metal Orthopaedic Implants*.* JBJS, 1998. **80**(2).
11. Sumitomo, N., et al., *Experiment study on fracture fixation with low rigidity titanium alloy: plate fixation of tibia fracture model in rabbit.* J Mater Sci Mater Med, 2008. **19**(4): p. 1581-6.
12. Niinomi, M., *Mechanical properties of biomedical titanium alloys.* Materials Science Engineering: A, 1998. **243**(1-2): p. 231-236.
13. Dutta, A., et al., *Design of porous titanium scaffold for complete mandibular reconstruction: The influence of pore architecture parameters.* Computers in Biology and Medicine, 2019. **108**: p. 31-41.

14. Orassi, V., et al., *In Silico Biomechanical Evaluation of WE43 Magnesium Plates for Mandibular Fracture Fixation.* Frontiers in bioengineering & biotechnology, 2022. **9**: p. 803103.
15. Barzegari, M., et al., *Computational modeling of degradation process of biodegradable magnesium biomaterials.* Corrosion Science, 2021. **190**.
16. Jahadakbar, A., et al., *Finite Element Simulation and Additive Manufacturing of Stiffness-Matched NiTi Fixation Hardware for Mandibular Reconstruction Surgery.* Bioengineering (Basel), 2016. **3**(4).
17. Moghaddam, N.S., et al., *Three Dimensional Printing of Stiffness-tuned, Nitinol Skeletal Fixation Hardware with an Example of Mandibular Segmental Defect Repair.* Procedia CIRP, 2016. **49**: p. 45-50.
18. Lee, P.Y., et al., *Comparison of Mechanical Stability of Elastic Titanium, Nickel-Titanium, and Stainless Steel Nails Used in the Fixation of Diaphyseal Long Bone Fractures.* Materials (Basel), 2018. **11**(11).
19. Aquilina, P., et al., *Finite element analysis of three patterns of internal fixation of fractures of the mandibular condyle.* British Journal of Oral Maxillofacial Surgery, 2013. **51**(4): p. 326-331.
20. Prasadh, S., et al., *Titanium versus magnesium plates for unilateral mandibular angle fracture fixation: biomechanical evaluation using 3-dimensional finite element analysis.* Journal of Materials Research and Technology, 2022. **18**: p. 2064-2076.
21. Jung, B.T., et al., *Biomechanical evaluation of unilateral subcondylar fracture of the mandible on the varying materials: A finite element analysis.* PLoS One, 2020. **15**(10): p. e0240352.
22. Gupta, A., et al., *Biomechanical influence of plate configurations on mandible subcondylar fracture fixation: a finite element study.* Medical & Biological Engineering & Computing, 2023.
23. Gupta, A., A. Dutta, and K. Mukherjee, *INFLUENCE OF PLATE DESIGN ON SUBCONDYLAR FRACTURE FIXATION: A COMPARATIVE FINITE ELEMENT ANALYSIS*, in *27th Congress of the European Society of Biomechanics*. 2022: Porto, Portugal.
24. Polgar, K., M. Viceconti, and J. Connor, *A comparison between automatically generated linear and parabolic tetrahedra when used to mesh a human femur.* Proceedings of the Institution of Mechanical Engineers, Part H: Journal of Engineering in Medicine, 2001. **215**(1): p. 85-94.
25. Dutta, A., et al., *Load transfer across a mandible during a mastication cycle: The effects of odontogenic tumour.* Proceedings of the Institution of Mechanical Engineers, Part H: Journal of Engineering in Medicine, 2020. **234**(5): p. 486-495.
26. Ichim, I., J. Kieser, and M. Swain, *Functional significance of strain distribution in the human mandible under masticatory load: numerical predictions.* Archives of Oral Biology, 2007. **52**(5): p. 465-473.
27. Meyer, C., L. Serhir, and P. Boutemi, *Experimental evaluation of three osteosynthesis devices used for stabilizing condylar fractures of the mandible.* Journal of Cranio-Maxillofacial Surgery, 2006. **34**(3): p. 173-181.
28. Hammer, B., P. Schier, and J. Prein, *Osteosynthesis of condylar neck fractures: a review of 30 patients.* The British journal of oral maxillofacial surgery, 1997. **35**(4): p. 288-291.
29. Choi, B.-H., C.-K. Yi, and J.-H. Yoo, *Clinical evaluation of 3 types of plate osteosynthesis for fixation of condylar neck fractures.* Journal of oral maxillofacial surgery, 2001. **59**(7): p. 734-737.
30. Osteonic. [cited 2022; Available from: https://osteonic.com/_brochure/Mandible%20Plating%20System.pdf.

31. Mukherjee, K. and S. Gupta, *Bone ingrowth around porous-coated acetabular implant: a three-dimensional finite element study using mechanoregulatory algorithm.* Biomechanics modeling in mechanobiology, 2016. **15**(2): p. 389-403.
32. Mukherjee, K. and S. Gupta, *The effects of musculoskeletal loading regimes on numerical evaluations of acetabular component.* Proceedings of the Institution of Mechanical Engineers, Part H: Journal of Engineering in Medicine, 2016. **230**(10): p. 918-929.
33. Mukherjee, K. and S. Gupta, *Mechanobiological simulations of peri-acetabular bone ingrowth: a comparative analysis of cell-phenotype specific and phenomenological algorithms.* Medical biological engineering computing, 2017. **55**(3): p. 449-465.
34. Dalstra, M., et al., *Mechanical and textural properties of pelvic trabecular bone.* Journal of biomechanics, 1993. **26**(4-5): p. 523-535.
35. Reina, J., et al., *Numerical estimation of bone density and elastic constants distribution in a human mandible.* Journal of Biomechanics, 2007. **40**(4): p. 828-836.
36. Manns, A., *Sistema estomatognático*. 1988.
37. Shockey, J., J. Von Fraunhofer, and D. Seligson, *A measurement of the coefficient of static friction of human long bones.* Surface Technology
1985. **25**(2): p. 167-173.
38. Chanda, S., et al., *A comparative assessment of two designs of hip stem using rule-based simulation of combined osseointegration and remodelling.* Proceedings of the Institution of Mechanical Engineers, Part H: Journal of Engineering in Medicine, 2019. **234**(1): p. 118-128.
39. O'Connor, C.F., R.G. Franciscus, and N.E. Holton, *Bite force production capability and efficiency in Neandertals and modern humans.* American Journal of Physical Anthropology: The Official Publication of the American Association of Physical Anthropologists, 2005. **127**(2): p. 129-151.
40. Korioth, T.W., D.P. Romilly, and A.G. Hannam, *Three-dimensional finite element stress analysis of the dentate human mandible.* American journal of physical anthropology, 1992. **88**(1): p. 69-96.
41. Pinheiro, M., et al., *Biomechanical evaluation of the human mandible after temporomandibular joint replacement under different biting conditions.* Sci Rep, 2021. **11**(1): p. 14034.
42. Moiduddin, K., et al., *Computer Assisted Design and Analysis of Customized Porous Plate for Mandibular Reconstruction.* Irbm, 2017. **38**(2): p. 78-89.
43. Perren, S., *Physical and biological aspects of fracture healing with special reference to internal fixation.* Clinical orthopaedics related research, 1979(138): p. 175-196.
44. Søballe, K., *Hydroxyapatite ceramic coating for bone implant fixation: mechanical and histological studies in dogs.* Acta Orthopaedica Scandinavica, 1993. **64**(sup255): p. 1-58.

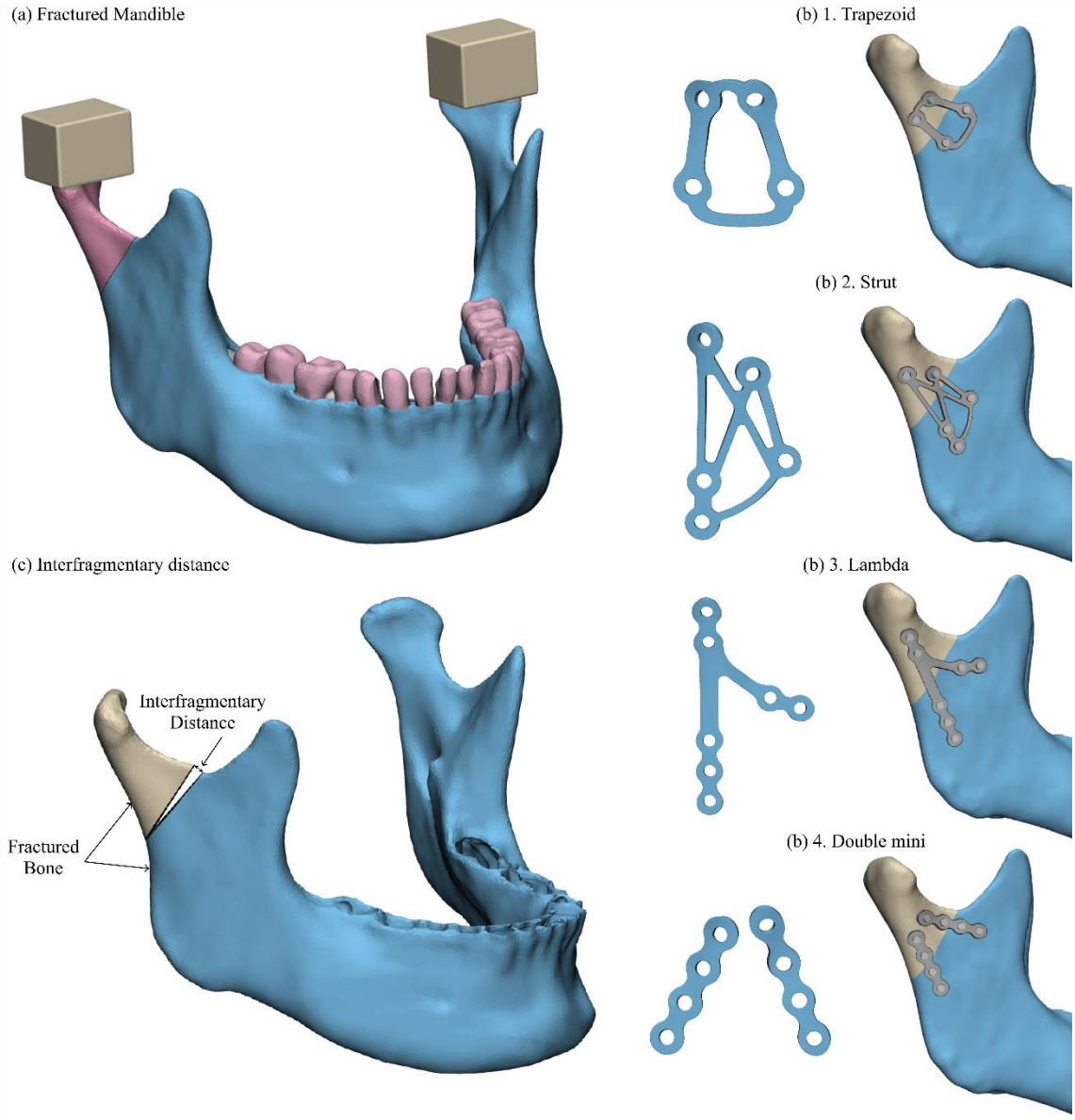

Figure 1. (a) Developed model of fractured mandible (b) Developed plate models and corresponding mandibular reconstructions: 1. Trapezoid, 2. Strut, 3. Lambda, 4. Double mini plates, (c) Interfragmentary distance calculated at the maximum opening end of the osteotomy site

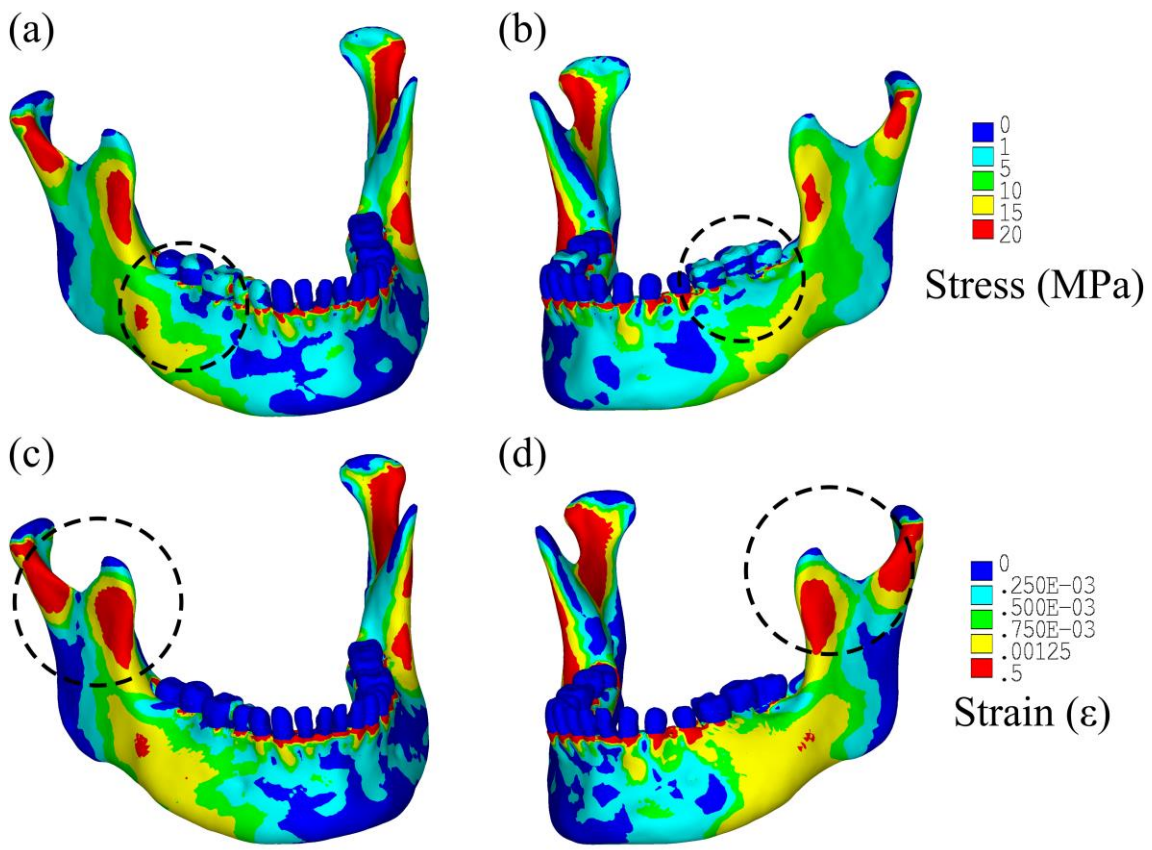

Figure 2. Principal tensile stress (top row) and strain (bottom row) distributions in intact mandible under (a, c) RMOL (b, d) LMOL

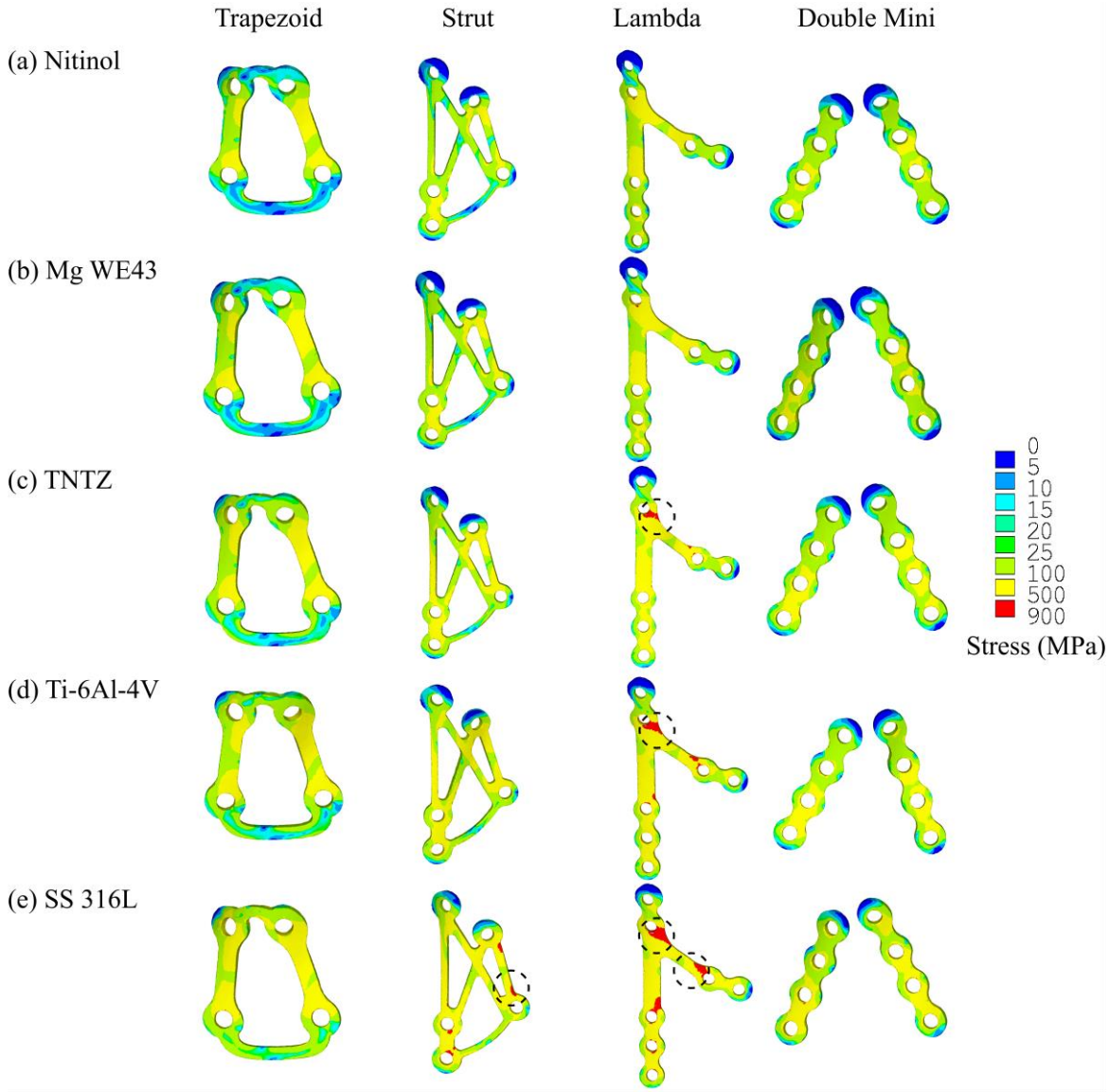

Figure 3. Equivalent von Mises stress distribution in trapezoid, strut, lambda and double mini plates for (a) Nitinol, (b) Mg WE43, (c) TNTZ, (d) Ti-6Al-4V and (e) SS 316L under RMOL

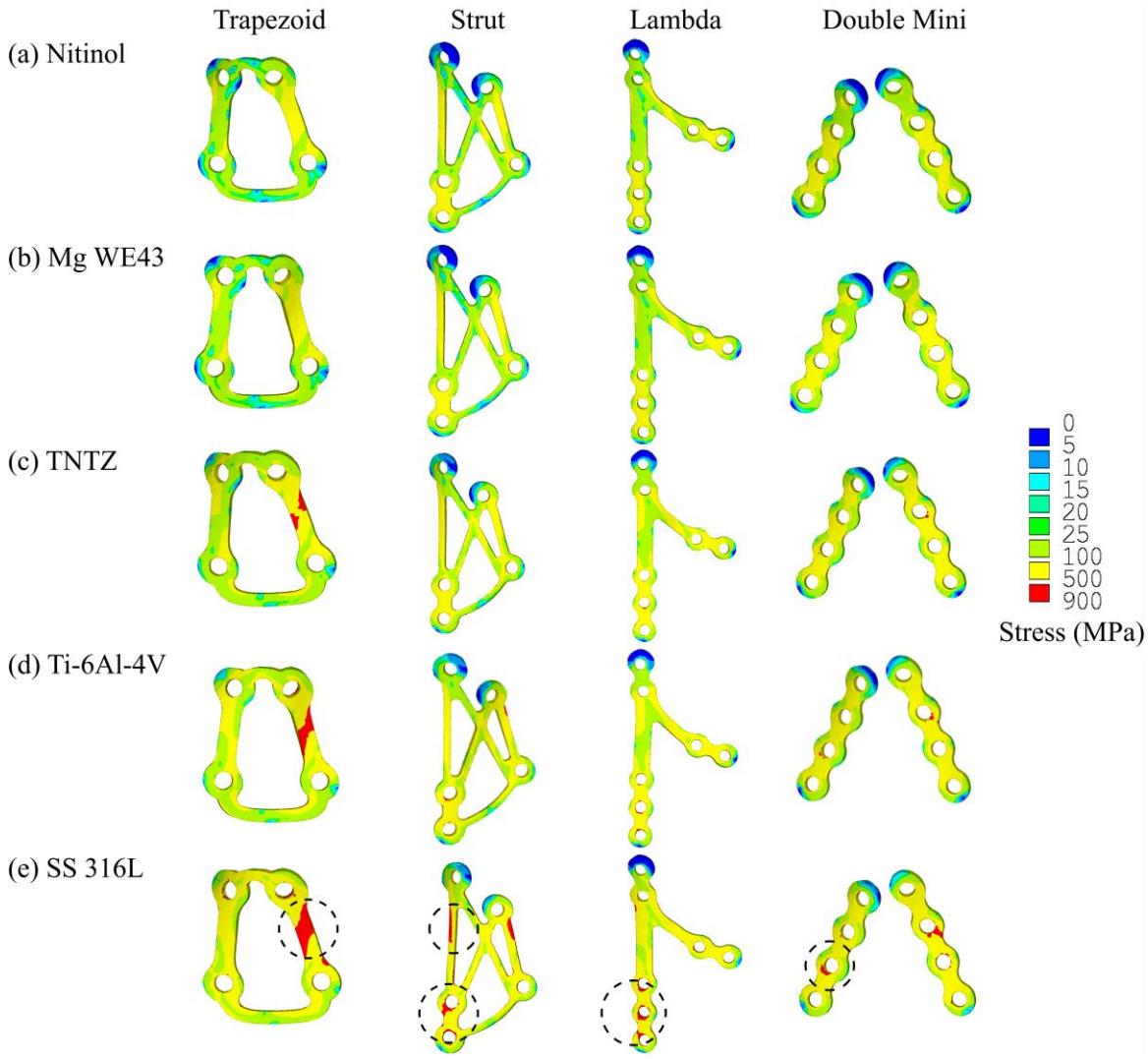

Figure 4. Equivalent von Mises stress distribution in trapezoid, strut, lambda and double mini plates for (a) Nitinol, (b) Mg WE43, (c) TNTZ, (d) Ti-6Al-4V and (e) SS 316L under LMOL

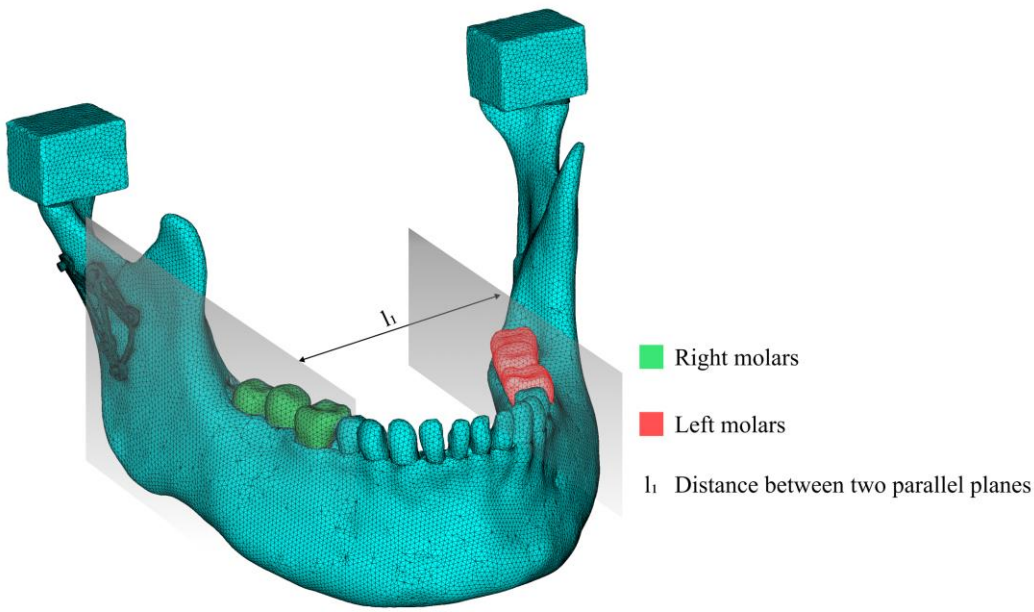

Figure 5. Plane passing through right molars and fracture site and plane through left molars

Table 1. Material properties of components of Finite Element Model

Component	E_X *(GPa)*	E_Y *(GPa)*	E_Z *(GPa)*	ν_{XY}	ν_{YZ}	ν_{XZ}	G_{XY} *(MPa)*	G_{YZ} *(MPa)*	G_{XZ} *(MPa)*
Symphysis and mental foramen	23	10	15	0.3	0.3	0.3	4800	3600	6200
Gonial angle	20	11	12	0.3	0.3	0.3	4800	5300	6000
Rest of cortical	17	6.9	8.2	0.3	0.3	0.3	2800	2900	4600
Cancellous	1×10^{-4} – 4.33	-	-	0.3	-	-	-	-	-
Enamel	80	-	-	0.3	-	-	-	-	-
Dentin	17.6	-	-	0.25	-	-	-	-	-
Condylar Fibrous Tissue	0.006	-	-	0.25	-	-	-	-	-
Periodontal ligament	0.003	-	-	0.45	-	-	-	-	-
Blocks	50000	-	-	0.3	-	-	-	-	-
Screws (Ti-6Al-4V)	110			0.3					

Table 2. Material properties of components of plates

Material	E_X ***(GPa)***	ν	***Yield Strength (MPa)***
Nitinol	38.5	0.3	200
Mg WE43	44.2	0.27	162
TNTZ	80	0.3	864
Ti-6Al-4V	110	0.3	900
SS 316L	210	0.3	380

Table 3. Maximum von Mises stresses (MPa) in plates during RMOL (Top row) and LMOL (Bottom row)

		Nitinol	Mg WE43	TNTZ	Ti-6Al-4V	SS 316L
RMOL	**Trapezoid**	143.50	149.68	184.76	213.56	299.79
	Strut	121.46	135.53	207.10	254.90	374.26
	Lambda	224.46	244.22	329.82	374.00	455.73
	Double mini	111.04	118.78	155.10	178.15	240.48
LMOL	**Trapezoid**	237.16	253.49	330.42	382.20	520.02
	Strut	185.87	204.78	298.50	358.37	497.99
	Lambda	170.62	187.50	264.48	315.83	449.15
	Double mini	205.18	217.11	269.26	302.33	383.64

Table 4. Interfragmentary distance (µm) during RMOL (Top row) and LMOL (Bottom row)

		Nitinol	Mg WE43	TNTZ	Ti-6Al-4V	SS 316L
RMOL	**Trapezoid**	17.96	18	18.11	18.12	18.08
	Strut	17.20	17.19	17.15	17.14	17.15
	Lambda	16.92	16.90	16.88	16.94	16.99
	Double Mini	17.77	17.74	17.63	17.29	17.51
LMOL	**Trapezoid**	116.9	112.60	92.56	80	68.40
	Strut	130.88	129.10	123.9	122	114.13
	Lambda	146	140.13	116.2	105.50	86.80
	Double Mini	44.90	42.17	31.40	26.50	18.70

Table 5. Maximum tensile strain (με) for reconstructed mandibles during RMOL (Top row) and LMOL (Bottom row)

		Nitinol	Mg WE43	TNTZ	Ti-6Al-4V	SS 316L
RMOL	**Trapezoid**	1605	1609	1614	1611	1595
	Strut	1541	1538	1528	1522	1517
	Lambda	1572	1568	1554	1549	1543
	Double mini	1635	1628	1603	1558	1569
LMOL	**Trapezoid**	6080	5642	3992	3301	2277
	Strut	4066	3175	2891	2474	1789
	Lambda	3554	3356	2653	2310	1738
	Double Mini	4452	4087	2845	2325	1493